European Journal of Medicinal Chemistry 54 (2012) 95–102

Contents lists available at SciVerse ScienceDirect

European Journal of Medicinal Chemistry

journal homepage: http://www.elsevier.com/locate/ejmech

Original article

Synthesis, crystal structures and electronic properties of isomers of chloro-pyridinylvinyl-1*H*-indoles

Laurence Moineaux [a,*], Sophie Laurent [b], Jérémy Reniers [a], Eduard Dolušić [a], Moreno Galleni [b], Jean-Marie Frère [b], Bernard Masereel [a], Raphaël Frédérick [a], Johan Wouters [a,**]

[a] Namur Medicine & Drug Innovation Center (NAMEDIC Member of NARILIS), Laboratory of Biological and Structural Chemistry, University of Namur (FUNDP), rue de Bruxelles 61, B-5000 Namur, Belgium
[b] CIP, ULg, Liège, Belgium

HIGHLIGHTS

- Three chloro-indolic isomers were synthesized and evaluated on hTDO.
- The single-crystal X-ray analyses of two of them revealed non-planar structures.
- The position of the Cl atom does not notably affect the electronic delocalization.
- The non-coplanarity plays a more important role in the crystalline packing.
- Physico-chemical properties led to an understanding of mechanism of TDO inhibition.

GRAPHICAL ABSTRACT

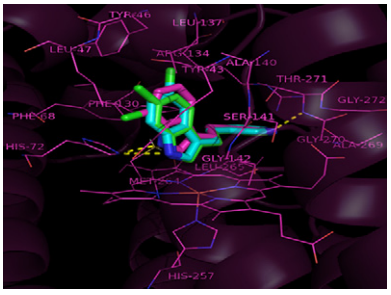

ARTICLE INFO

Article history:
Received 15 November 2011
Received in revised form
30 March 2012
Accepted 24 April 2012
Available online 3 May 2012

Keywords:
Chloro-3-(2-pyridin-3-ylvinyl)-1*H*-indole
Human tryptophan 2,3-dioxygenase
Physico-chemical properties
Crystal structure
Isomer

ABSTRACT

Three isomers of chloro-3-(2-pyridin-3-ylvinyl)-1*H*-indole were synthesized and tested as inhibitors of human tryptophan 2,3-dioxygenase (hTDO). The crystal structures of two of them were solved by X-ray diffraction. The solubility of the molecules also was determined experimentally. The molecular electrostatic potentials and dipole moments of the three isomers were calculated by *ab initio* quantum mechanics (HF/6-311G).

The single crystal X-ray analyses reveal non-planar structures. This non-coplanarity is retained during docking of the compounds into a model of hTDO, the molecular target of this series. The position of the Cl atom does not significantly affect the electronic delocalization. Nevertheless, the position of the Cl atom produces a local variation of bond lengths inducing different dipole moments for these isomers. Variations in dipole moments are consistent with the different melting points and crystal packings. Differences in aqueous solubilities are best explained by subtle changes in H-bonds resulting from different accessibilities of the indole NH's due to steric effects of the Cl substituent. The non-coplanarity plays an important role in the crystalline packing of the molecules in contrast to the position of the Cl. This study leads to a better understanding of the structural and electronic characteristics of this chemical series and can potentially help to better understand their inhibitory activity.

1. Introduction

The essential amino acid L-tryptophan (L-Trp) is required for the biosynthesis of proteins and is a precursor for several biologically

* Corresponding author. Tel.: +32(0)81724569.
** Corresponding author.
E-mail addresses: Laurence.moineaux@fundp.ac.be (L. Moineaux), johan.wouters@fundp.ac.be (J. Wouters).

0223-5234/$ – see front matter © 2012 Elsevier Masson SAS. All rights reserved.
doi:10.1016/j.ejmech.2012.04.033

important compounds, including 5-hydroxytryptamine (5-HT, serotonin), kynurenic acid or nicotinamide [1–3]. Tryptophan hydroxylase controls 5-HT synthesis in the brain. In fact, this enzyme has a large capacity for processing its substrate, tryptophan, and it has been shown that higher brain tryptophan levels cause an increase in the 5-HT levels in both whole-brain and brain extracellular fluid. Indeed, L-tryptophan may be used as an antidepressant but its efficacy is weak because of its rapid catabolism [4].

The L-kynurenine pathway is the major catabolic route of L-tryptophan metabolism and the key controlling enzymes are tryptophan 2,3-dioxygenase (TDO) and indoleamine 2,3-dioxygenase (IDO). Both are cytosolic heme dioxygenases that catalyze the oxidative cleavage of the C_2–C_3 bond of the indole ring of L-tryptophan. This reaction is the first and rate-limiting step of the kynurenine pathway of tryptophan catabolism, which eventually leads to the formation of nicotinamide dinucleotide (NAD^+), a process regarded as the primary biological function of TDO [5–8]. Although hTDO and hIDO catalyze the same reaction and share relatively conserved active site regions, amino acid sequences do not exhibit more than a 10% level of identity [9], their physiological functions are distinct. TDO is homotetrameric and almost exclusively found in the liver [10]. It is highly specific for L-tryptophan and some of its derivatives substituted in the 5- and 6-positions of the indole ring [11]. On the other hand, IDO is monomeric and extrahepatic and shows activity toward a larger collection of substrates, including serotonin, tryptamine, 5-hydroxytryptophan, and melatonin. The two enzymes also have different inducers; IDO is induced by inflammatory stimuli such as interferon-γ, and TDO by tryptophan, glucocorticoids, and kynurenine [7,12].

Kynurenine pathway metabolites have been implicated in a number of diseases ranging from neurological disorders, such as cerebral malaria and multiple sclerosis, to cataract formation [13,14]. Recent findings have implicated IDO-mediated tryptophan catabolism in immune tolerance, including immune suppression in maternal fetal tolerance and the immune escape of cancers [15–20].

While IDO is a well-established target for cancer immunotherapy [21–28], it was only recently reported that TDO is also expressed in many tumor cells including melanoma, colorectal, bladder, hepatic, breast and lung cancers in a murine model of cancer [29]. This work demonstrated that TDO expression in tumors has an effect similar to the expression of IDO, preventing tumor rejection by locally degrading tryptophan. A recent study confirmed another important mechanism of TDO-mediated tumoral immune suppression, namely the release of the tryptophan catabolite kynurenine, which then binds to the aryl hydrocarbon receptor (AHR) [30]. Recently, we contributed to a study describing a small-molecule TDO inhibitor which enables reversal of tumoral immune resistance *in vivo* [31]. These findings underline the importance of the precise TDO catalytic mechanism and fully justify the search for potent inhibitors.

Until recently, only a handful of compounds based on the indole or β-carboline scaffolds were reported as exhibiting TDO inhibitory activity [5,32–35]. Among these, fluoroindoles (**680C91** and **709W92**, Fig. 1) [5,34,35] belonging to the 3-(2-(pyridyl)ethenyl) indole class described by the Wellcome group as combined TDO/5-HT (serotonin) reuptake inhibitors for antidepressant therapy seemed to be the most interesting hits. **680C91** is an excellent *in vitro* inhibitor (K_i of around 30 nM) on liver-extracted TDO, and at 10 μM, has no activity on 5-HT reuptake, various 5-HT receptors, IDO and monoamine oxidases A and B [35]. However, *in vivo*, the compound has no pronounced effect on tryptophan levels in rat, presumably because of bioavailability/metabolism problems [31,36,37].

As part of our interest in the design and synthesis of original TDO inhibitors [38], we describe in this paper the structure and physico-chemical properties of three isomers of chloro-pyridinylvinyl-1*H*-indole, confirm they inhibit TDO and propose a rationale for this inhibition by docking simulations.

2. Experimental section

2.1. Single X-ray diffraction

Crystals of all three ((*E*)-chloro-3-(2-pyridin-3-ylvinyl)-1*H*-indoles) were obtained by slow evaporation of solutions of the samples at room temperature. Only crystals of (**1**) and (**3**) allowed good quality structure determination by crystallography. X-ray measurements were performed on a Gemini Ultra R system (4-circle kappa platform, Ruby CCD detector) using Mo Kλ radiation ($\lambda = 0.71073$ Å). After mounting and centering the single-crystal on the diffractometer, cell parameters were estimated from a pre-experiment run and full data sets were collected at room temperature. Structures were solved by direct methods with the SHELXS-97 program and then refined on F^2 using the SHELXL-97 software [39]. E-map provided positions for all non H-atoms. The full-matrix least-squares refinement was carried out on F^2 using anisotropic temperature factors for all non H-atoms. The H-atoms were located from ΔF-maps, and then their positions were refined using a riding model with isotropic thermal parameters taken as 1.2 times temperature factors for their parent-atoms. The ORTEPs of these isomers were obtained by the PLATON [40] program.

The quality of the crystallographic data for 6-chloro-3-(2-pyridin-3-ylvinyl)-1*H*-indole was too poor to allow a good structure determination.

Crystal data for (**1**): crystallization by slow evaporation from a toluene–methyl acetate solution (1:1). Crystal dimensions: 0,20 × 0,10 × 0,28 mm. Monoclinic *C*2/*c*, $a = 15.784(2)$ Å, $b = 9.352(1)$ Å, $c = 17.080(2)$ Å, $V = 2492.3(5)$ Å, $Z = 8$, $D_{calc} = 1.3576$ g/cm^3, μ(Mo Kλ) = 0.288 mm^{-1}, $F(000) = 1056$, $\theta_{min} = 3.4°$ to $\theta_{max} = 27.9°$, $R = 0.0344$, $wR2 = 0.072$, observed data ($I > 2\sigma I$) = 1257, total = 2599, R(int) = 0.035, $S = 0.793$.

Crystal data for (**3**): crystallization by slow evaporation from a toluene–ethyl acetate solution (1:1). Crystal dimensions: 0,20 × 0,40 × 0,35 mm. Triclinic *P*−1, $a = 11.081(1)$ Å, $b = 13.128(1)$ Å, $c = 14.863(1)$ Å, $V = 1862.9(3)$ Å, $Z = 6$ (3 molecules in the a.u.), $D_{calc} = 1.3623$ g/cm^3, μ(Mo Kλ) = 0.289 mm^{-1}, $F(000) = 792$, $\theta_{min} = 3.3°$ to $\theta_{max} = 32.6°$, $R = 0.0636$, $wR2 = 0.119$, observed data ($I > 2\sigma I$) = 4184, total = 12,288, R(int) = 0.05, $S = 0.845$.

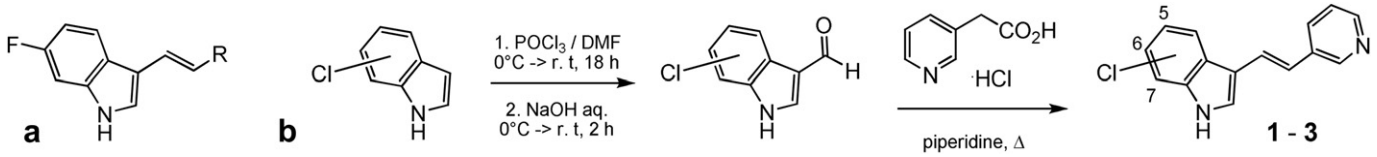

Fig. 1. a, Structures of the leads. **680C91**: R = pyrid-3-yl; **709W92**: R = pyrid-4-yl; b, general synthetic procedure for chloro-pyridinylvinlyl-1*H*-indoles. (**1**), 5-Cl; (**2**), 6-Cl; (**3**), 7-Cl-isomer.

2.2. Computational methods

In order to model the structure, geometry optimization was performed at the rhf/6-311G level of theory using the *Gaussian* suite of programs [41]. Molecular electrostatic potential (MEP), suppress HOMO–LUMO topologies and energies, and dipole moment were computed. *Gaussview* allowed the visualization of dipole moments, suppress HOMO–LUMO topologies and MEPs.

2.3. Solubility evaluation

The solubility was evaluated using Multiscreen HTS-PCF filter plates from Millipore according to a protocol adapted from the Millipore application note ("Quantitative method to determine drug aqueous solubility: optimization and correlation to standard methods" Thomas Onofrey and Greg Kazan http://www.millipore.com/techpublications/tech1/an1730en00) at pH 1.0 (HCl 0.1 M, NaCl 20 mM), 7.4 (phosphate buffer 50 mM, NaCl 30 mM) and 9.0 (boric acid 0.1 M, NaCl 20 mM) and with a final DMSO concentration of 2.5%. The filtrate was analyzed using an Agilent 1100 Series LC/MSD Trap system with UV detection at 254 nm equipped with a C18 Zorbax SB column (100 × 3 mm; 3.5 μm) and following a gradient (flow rate: 0.5 mL min^{-1}) of acetonitrile in aqueous acetic acid 0.1% (v/v) (gradient: from 5 to 95% of acetonitrile in 5 min, holding for 3 min, then reversing to 5% of acetonitrile in 0.1 min and holding for an additional 5.4 min).

2.4. IC_{50} determination on hTDO

Enzymatic assays were performed by measuring the rate of kynurenine formation by a discontinuous colorimetric method. The reactions were performed by adding 1.3 μM (100 μl) purified human TDO (hTDO) in a reaction mixture (900 μl) containing 50 mM tris buffer pH 8.0, 20 mM ascorbic acid, 100 μg of Bovine Liver catalase, 5 μM hemin, 10 μM methylene blue, 100 μM L-tryptophan and different concentrations of potential inhibitors in a range of 0–100 μM. The mixture was pre-incubated at 37 °C for 10 min before addition of the enzyme. The reactions were stopped after 5, 10, 15 or 20 min by adding 40 μl of 30% trichloroacetic acid to 200 μl of the reaction mixture and further incubated at 65 °C for 15 min to hydrolyze *N*-formylkynurenine into kynurenine. After centrifugation at 19,300 *g* for 10 min, 100 μl of supernatant were added to 100 μl of *para*-dimethylaminobenzaldehyde (Ehrlich's reagent) in a 96-well plate. A positive reaction yields a yellow solution [42]. The amount of formed kynurenine was determined spectrophotometrically at 480 nm. Data were analyzed with the GraphPadPrism 5.0 program [43]. All determinations were performed in duplicate and the presented data are average values.

The solutions and dilutions of the different inhibitors were prepared in 100% DMSO. The final concentration of DMSO in the assay mixture was 5% and it was verified that this concentration did not affect the enzymatic activity. The enzyme studied is a recombinant form of human tryptophan 2,3-dioxygenase (hTDO) produced in *Escherichia coli* and purified to homogeneity.

2.5. Molecular modeling

Sequence alignment between human TDO (obtained from the Swiss-Prot database) [44] and *Ralstonia metallidurans* (rmTDO (PDB code 2NOX)) [45] was performed using BLASTP [46–48]. A model of human TDO was thus developed by *in silico* mutation of only a few amino acids from rmTDO. To take into account protein flexibility, the resulting model was minimized using the MINIMIZE module included in SYBYL 8.0 program [49].

Molecular modeling studies were carried out on a Linux workstation. The compounds were built using the SKETCH module implemented in SYBYL (version 8.0) [49]. Docking was performed using the 3D coordinates of our humanized TDO model with the help of the automated GOLD program [50] (active site definition: residues within 10 Å around heme). In order to take protein flexibility into account, the enzyme–inhibitor complexes were optimized using the MINIMIZE module. The minimization process uses the Powell method with the Tripos force field (dielectric constant 1*r*) to reach a final convergence of 0.01 kcal mol^{-1}.

3. Results and discussion

3.1. Compound synthesis

The compounds were synthesized according to the procedure described in Fig. 1 and detailed elsewhere [38].

3.2. IC_{50} determination on human TDO

IC_{50} values were determined for two isomers of chloro-3-(2-pyridin-3-ylvinyl)-1*H*-indole on the purified human TDO. For isomers (**1**) and (**2**), the IC_{50} values were 10 ± 0.5 μM and 5 ± 0.4 μM respectively (Fig. 2).

For isomer (**3**), concentrations higher than 50 μM could not be obtained because of solubility problems so that it was not possible to determine an IC_{50} value by the same method. Thus, a K_i value was determined by varying the substrate and inhibitor concentrations

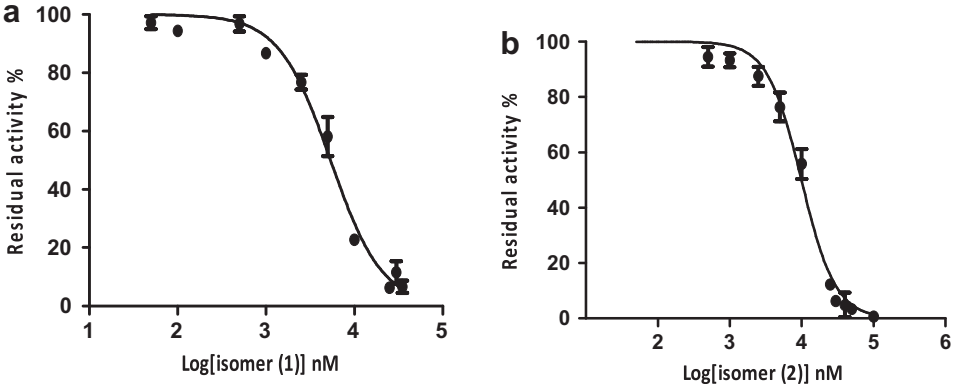

Fig. 2. Residual activity (%) of purified human TDO in presence of isomers (**1**) (a) and (**2**) b. The enzymatic assays were performed in duplicate as described in the Experimental section.

and fitting the data to the Henri–Michaelis–Menten equation (Fig. 3). This study showed that isomer (**3**) behaved as a competitive inhibitor with a K_i value of 21 ± 0.3 μM. On the basis of the same data, the K_m value was evaluated at 180 ± 1.4 μM, in good agreement with the value determined in the absence of inhibitor.

To compare with the other two isomers, an IC_{50} value was calculated with the help of the Dixon equation [51] for competitive inhibition (Equation (1)).

$$IC_{50} = K_i\left(1 + \frac{S}{K_m}\right) \quad (1)$$

At a substrate concentration of 100 μM, the calculated IC_{50} is 32 ± 0.02 μM. The inhibitory activity is thus lower than that of the other two isomers. This is consistent with the docking analysis (see Sec. 3.6).

The three isomers inhibited hTDO and the best inhibitory activity was obtained with the chlorine atom in position 5 on the indole ring (**1**). However, these isomers of the chloro-pyridinylvinyl-1*H*-indole family do not exhibit better inhibitory activities than the reference inhibitor 680C91 (IC_{50} near 1.3 μM).

3.3. Molecular conformation

Only a very limited number of substituted vinyl-1*H*-indoles (*e.g.* 3-(2′-nitrovinyl)indole (CSD code: GOJDUE), ethyl 3-(1*H*-indol-3-yl)acrylate (CSD code: GUGLEA), 3-(3-indolyl)acrylamide (CSD code: SUVYIR), or (*E*)-4-(3-indolylvinyl)-*N*-methylpyridinium iodide (CSD code: TIKBEU and TIKBIY)) crystal structures have been determined by crystallography. Efforts to obtain crystals of fluoro-substituted 3-(2-pyridin-3-ylvinyl)-1*H*-indole isomers, including 680C91 proved unsuccessful in our hands. In contrast, crystals of chloro-substituted 3-(2-pyridin-3-ylvinyl)-1*H*-indoles could be grown providing valuable structural information on this family of compounds both in terms of in depth analysis of molecular conformations and crystal packings but also serving as starting point for geometry optimizations.

Fig. 4 shows the ORTEP diagram of 5- and 7-chloro-3-(2-pyridin-3-ylvinyl)-1*H*-indole isomers ((**1**) and (**3**), respectively) with the atom numbering scheme. There are three molecules in the asymmetric unit of (**3**) in contrast to (**1**).

Both compounds possess an *E* configuration at the C(10)=C(11) double bond. Unexpectedly, this study reveals a significant deviation from coplanarity. Indeed, the values of the dihedral angle between the plane of the pyridine and that of the indole are:

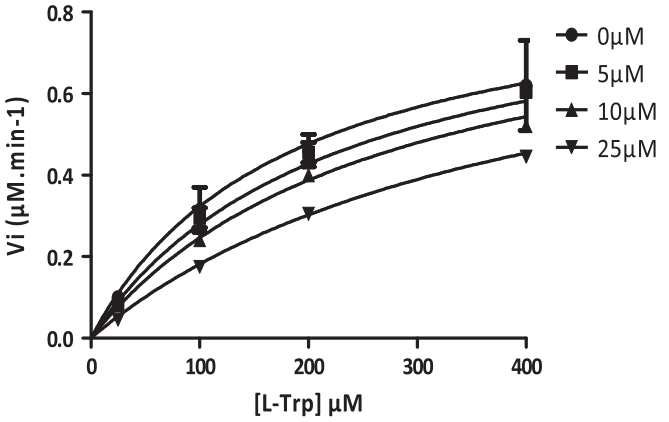

Fig. 3. Initial rate of L-Trp oxidation by purified hTDO in the presence of varying concentrations of 7-chloro-3-(2-pyridin-3-ylvinyl)-1*H*-indole (**3**) and L-Trip. The enzymatic assays were performed as described in the Experimental section.

46.49(7)° (**1**), 22.23(7)° (**3a**), 19.01(5)° (**3b**), and 17.17(5)° (**3c**). Table 1S gives values of selected bond lengths for the two isomers. These geometries obtained by crystallography (crystal packing effects) are retained in structures optimized by *ab initio* methods (rhf/6-311G) (Table 1S, supplementary data and tables for this paper are available from supplementary materials). Influence of the position of the Cl atom in the two isomers is essentially limited to the C(4)–C(5), C(5)–C(6) and C(6)–C(7) bond lengths. Optimization of (**3**), starting from the three distinct conformers (**a**, **b**, **c**) observed in the crystal structure converged to a unique structure.

3.4. Crystal packing and intermolecular interactions

The crystal packings of (**1**) and (**3a**, **b**, **c**) are essentially determined by two factors: π-stacking and hydrogen bonds (HB).

For both isomers (**1**) and (**3**), a strong HB links nitrogen (N3′) of pyridine (hydrogen bond acceptor, A) with the (N1–H1) of the indole ring (H-bond donor, DH) of a symmetry-related molecule (Fig. 5). The isomers (**3a**) and (**3b**) exhibit a weak HB between nitrogen (N3′) of the pyridine and the (C1–H1) of the indole ring [53,54]. The total number (one D–H and one A per molecule) and strength (reflected by d, Table 2S, [52]) of these H-bonds is similar for both isomers. Geometrical parameters used to describe the stacking interactions are defined in Table 3S which lists the values of these parameters for our 2 crystal structures.

The crystal packing modes of compounds (**1**) and (**3**) are given in Fig. 5. In the packing of compound (**1**), the 6-membered ring of the indole interacts with the 5-membered ring of another indole moiety by π–π stacking interactions. There is an additional π–π interaction between the pyridine group and the indole ring. In contrast, for compound (**3**), only the 6-membered rings of the indoles interact.

It is tempting to compare the stabilizing effects of crystal packing with experimental physico-chemical parameters of the compounds, in particular melting points (mp) [55] and solubility. Therefore, melting points were determined. The solubility was evaluated using Multiscreen HTS-PCF filter plates from Millipore (Table 1).

Indeed, several H-bond interactions in (**3**) are similar to those in compound (**1**) but analysis of the crystal packing suggests that π–π interactions are stronger for (**1**). This is consistent with the melting points of these compounds. Compound (**1**), in which there is a better stabilization by π-stacking, has a higher mp (222–223 °C) than compound (**3**) (204–205 °C) with weaker stacking interactions and similar H-bonds. It can be anticipated that the crystal packing of (**2**) would be closer to that of (**3**) than to that of (**1**).

Aqueous solubility of the compounds (Table 1) is related to both the stability of the solid state packing and solvation effects. If one refers to the stability of the solid solutes (similar H-bonds and differences in π-interactions) used to explain the experimental melting points, the solubilities of (**1**) and (**3**) cannot be easily explained. Indeed, compound (**1**), with the stronger packing (and higher mp), is also more soluble that (**3**) (23 mg/mL for (**1**) compared to 2.3 mg/mL for (**3**) at pH 7.4). The lower solubilities (at pH 7.4 and 9.0) must thus be explained by solvation effects. As discussed further (point 3.5.2 MEP) the position of the chlorine atom close to the indole NH limits access to the H-bond donor and significantly stabilizes interactions with water molecules. This steric effect of the Cl atom, which affects aqueous solubility (mediated by H-bonding to the indole NH) could also explain, in part, the lower affinity of (**3**) for TDO.

The solubility of this series of compounds is higher at low pH (a 20 fold increase of solubility of (**1**) between pH 7.4 and pH 1). This is most probably explained by protonation of the pyridine ring at low pH values.

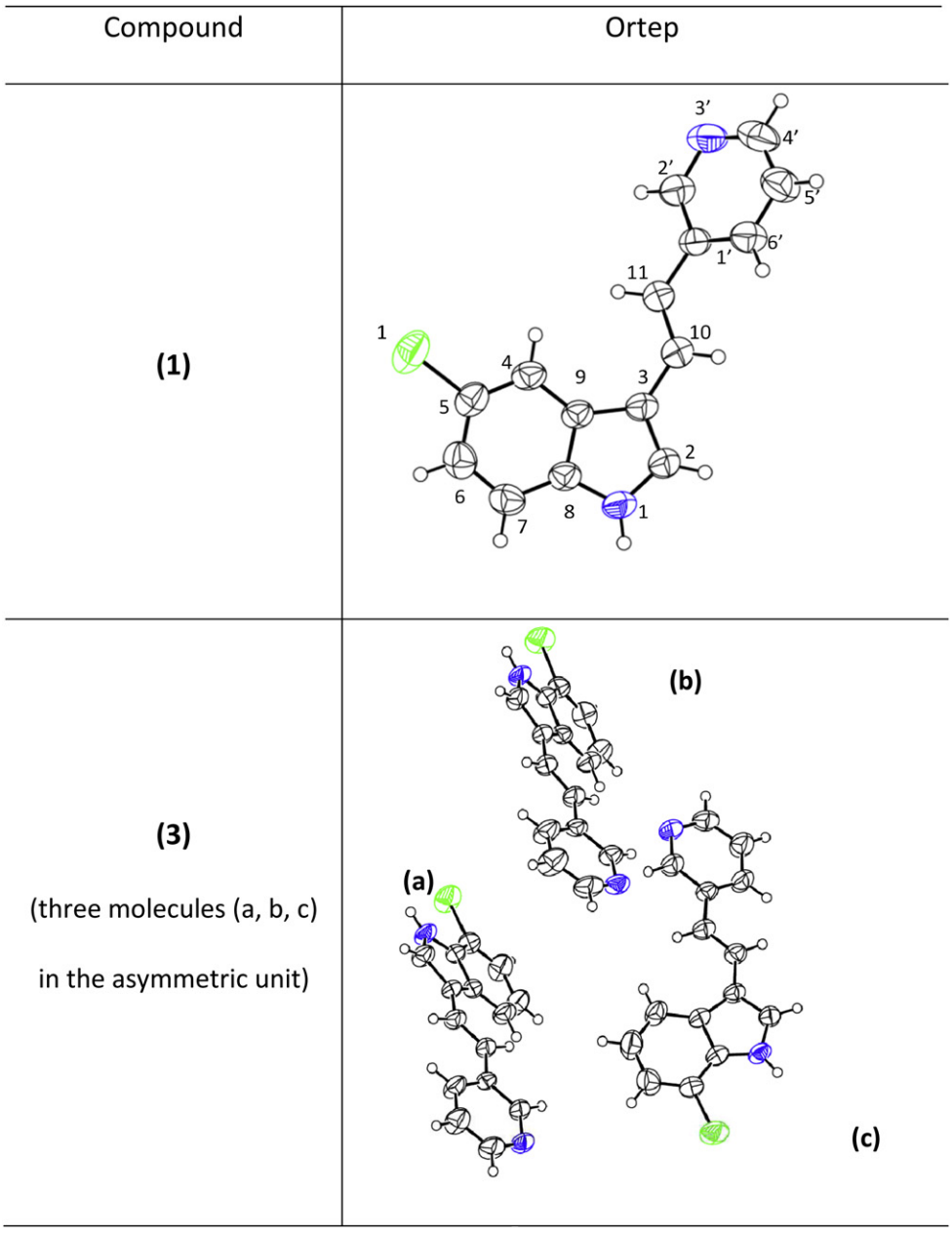

Fig. 4. View of the crystal structure conformations (ORTEP diagram, 50% probability level) for compounds (**1**) [top] and (**3**) [bottom]. Numbering is the same for all the molecules. There are three molecules (a, b, c) in the asymmetric unit of (**3**).

3.5. Electronic properties

3.5.1. Dipole moments

The molecular dipole moment is a measure of charge distribution in a molecule. The accuracy of the overall distribution of electrons in a molecule is difficult to quantify, since it involves all the multipoles. From the present calculations, the total dipole moment and orientation vectors calculated with the geometries optimized at the rhf/6-311G level of theory are given in Table 1.

The variations in the dipole moments are consistent with the different melting points of the solids and to some extent, with their solubility. Correlation with the solubility is less clear, as already noted by others [56].

The influence of the position of the Cl substituent on the distribution of atomic charges is limited but nevertheless leads to significant variations in the molecular dipole moments (Fig. 6a, Table 1). Compounds (**1**) and (**2**) exhibit a molecular dipole moments larger than that of compound (**3**).

This is in agreement with similar H-bond patterns (in the crystal packing) but distinct orientations of the molecule (due to the π−π stacking of the rings) in the crystal.

3.5.2. Electrostatic potential around isolated molecules

In order to calculate the molecular electrostatic potentials (MEP) of these molecules, the geometry of the system was first optimized at the rhf/6-311G level of theory. Secondly, mapping of the MEP onto the molecular surface was performed with Gaussview. The MEP maps (Fig. 4b) reveal that essentially all three non charged molecules present similar topologies and charge distributions. All three compounds are characterized by attractive (negative) potentials (red–yellow) on the N atom of the pyridine and a positive potential (blue) on the N–H function of the indole ring. The Cl

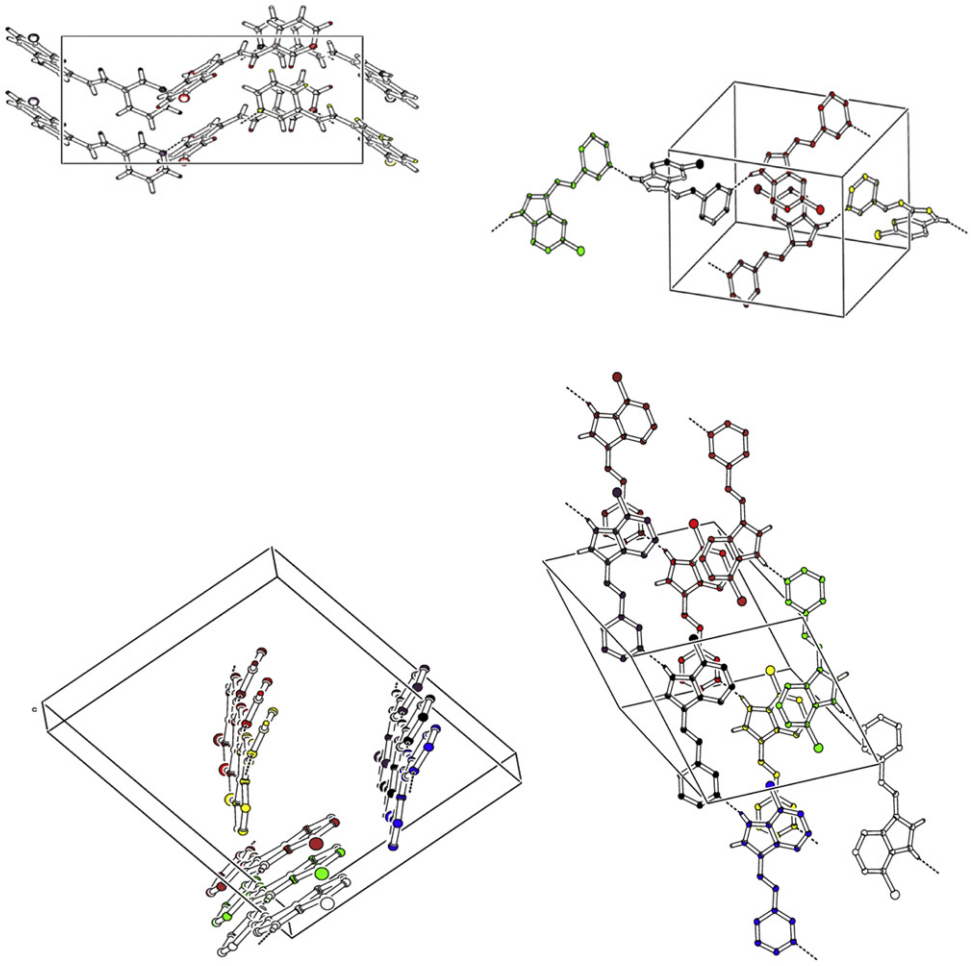

Fig. 5. Views of the crystal packing of (**1**) [top] and (**2**) [bottom]. Two selected orientations of the cell are presented for each compound in order to better visualize both hydrogen bonds (highlighted by dotted lines) and π-stacking interactions.

atom also contributes and generates some attractive potential but to a much lesser extent than the nitrogen of the pyridine.

This topology is in agreement with the H-bonds determined in the crystallographic structure. Indeed, the pyridine nitrogen (N3′) is an H-bond acceptor which corresponds to the basic (negative) site in MEP and the (N1–H1) of the indole group is an H-bond donor which corresponds to the most positive region of the MEP. Interestingly, as already underlined in the discussion of aqueous solubility of our series, the relative position of the chlorine substituent has a direct effect (steric hindrance and 'shading') on the MEP and in consequence on the ability of the three isomers to form H-bonds.

Table 1
Physico-chemical parameters of (**1**), (**2**) and (**3**): experimental properties (melting points and solubilities determined at 3 pH's) and calculated (rhf/6-311G) electronic properties (molecular dipole moment).

Compound	(**1**)	(**2**)	(**3**)
Solubility (mg/mL)			
pH 1	540.3	473.3	550.8
pH 7.4	23.0	22.3	2.3
pH 9	76.0	32.1	6.0
Molecular dipole moment (D)	7.41	5.69	3.15
Orientation vector of dipolar moment (*x*,*y*,*z*)	−1.61; −7.18; 0.86	0.43; 5.61; 0.80	0.32; −2.93; 1.12
Melting point (°C)	222–223	204–208	204–205

3.6. Modeling and docking

The biological data and stereo-electronic properties derived from our study of the title compounds were combined with docking simulations into the active site of TDO and proved useful to better understand the TDO inhibitory activity of those molecules.

To date, only the 3-D coordinates of TDO from *R. metallidurans* (rmTDO) (PDB code: 2NOX) [45] and *Xanthomonas Campestris* (xcTDO) [9] (PDB code: 1YW0) have been experimentally obtained. These two bacterial TDOs present high sequence similarities with the human form (28–34%) and excellent identities in the catalytic site area. Sequences of hTDO and rmTDO were aligned using the BLASTP program [46–48], showing that amino acids essential to the activity were well preserved around the heme cofactor. Docking of the three isomers in the active site was performed in the structure of humanized rmTDO (i.e.: hTDO residues were mutated in the structure of rmTDO) using the GOLD program [50]. The results are summarized in Fig. 7.

The geometries of the three isomers in the docking solutions are consistent with the crystallographic structures. Indeed, the non-coplanarity, and the *trans* configuration observed in the crystallographic study of these compounds is retained in the docking. Moreover, the essential binding points (HB interactions and π-stacking interactions) are also observed between the inhibitors and the active site residues of TDO, for example, the formation of H-bonds between the –NH of indole and His 72 and between the

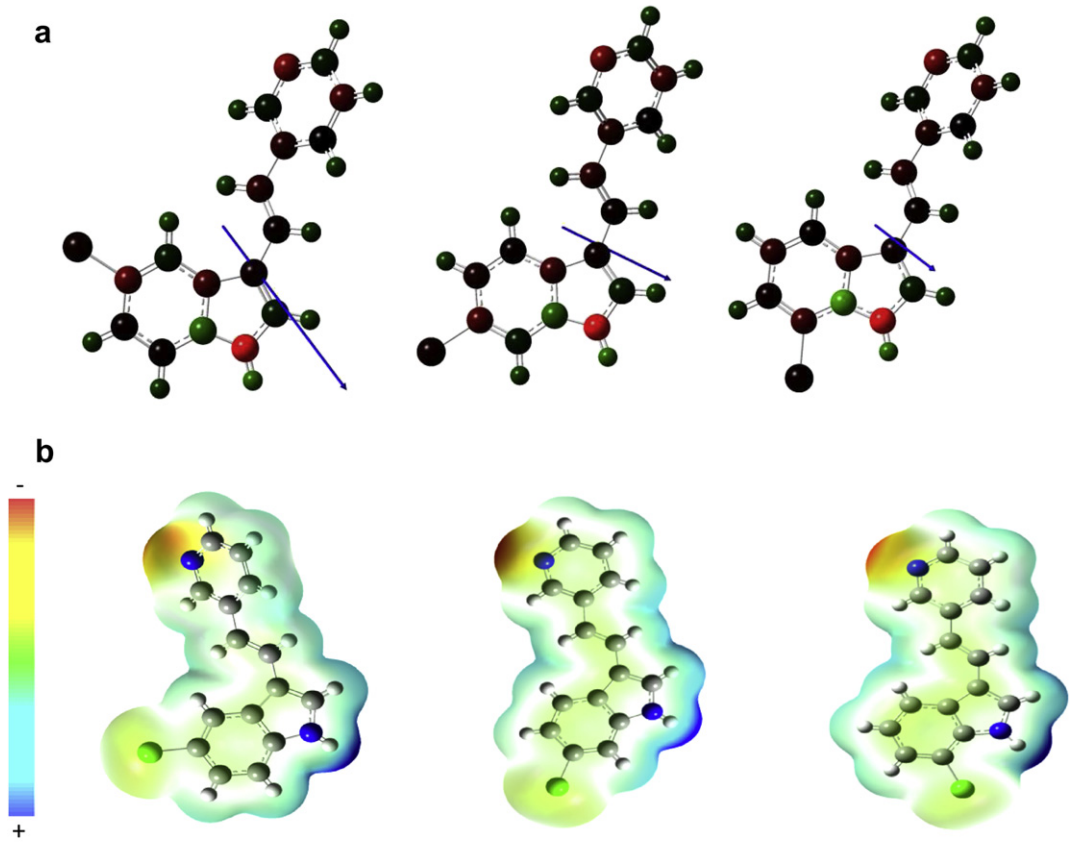

Fig. 6. Representation of selected electronic properties calculated (rhf/6-311G) on optimized geometries of (**1**) [left], (**2**) [middle] and (**3**) [right]: molecular dipole moments (a, top) and MEP contours (range between 179 and 179 kcal/mol, b, bottom).

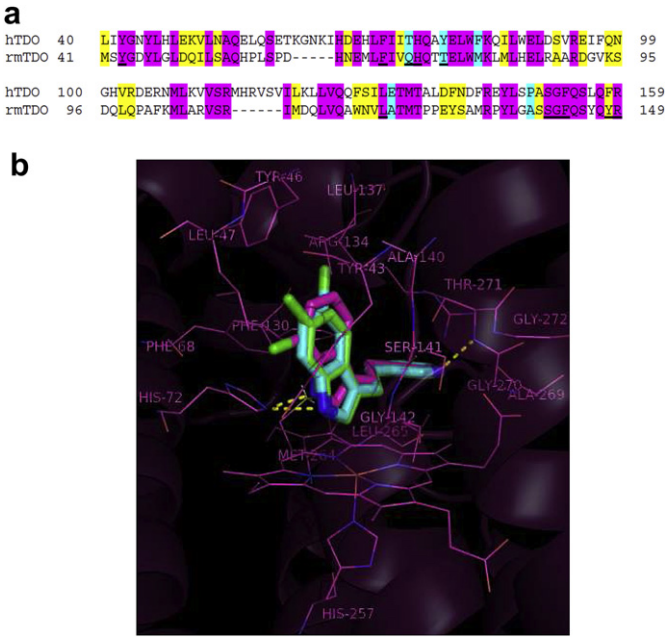

Fig. 7. (a, top), Sequence alignment used for modeling of hTDO: residues of catalytic site area (4 Å, underlined), conserved residue (pink), similar residues (yellow) and different residues (blue) and (b, bottom) docked structure of (**1**) (blue), (**2**) (green) and (**3**) (pink) into the active site of rmTDO.

nitrogen of pyridine and Thr 271. These hydrogen bonds are similar to those observed in the crystallographic study performed on the two (isolated) isomeric chloro-3-(2-pyridin-3-ylvinyl)-1*H*-indoles. These molecules interact in the same way as the reference inhibitor (**680C91**) [38].

Based on the docking simulations, it is tempting to suggest that the reduced inhibition of TDO by compound (**3**) is due to a significant displacement of this inhibitor, compared to molecules (**1**) and (**2**) which overlap well. This displacement, induced by steric effects caused by the Cl atom, could result in a less favorable HB interaction with His 72. In addition, the significantly reduced value of the dipole moment of (**3**) versus (**1**) and (**2**) could also explain weaker $\pi-\pi$ interactions within the active site of TDO and thus a reduced affinity for the enzyme. This is consistent with the IC_{50} analysis.

4. Conclusions

In conclusion, the TDO inhibition potencies of three previously synthesized isomers of chloro-3-(2-pyridin-3-ylvinyl)-1*H*-indole were evaluated. The single-crystal X-ray analyses of two of them revealed non-planar structures. This non-coplanarity is retained during docking of the compounds into the active site of a model of human TDO. The position of the Cl atom does not significantly affect the electronic delocalization within the molecule but allows local bond length variations and overall differences for the value and orientation of the dipole moments. Variations in dipole moments are consistent with different melting points and crystal packings. Differences in aqueous solubilities are best explained by subtle

changes in H-bonds resulting from different accessibilities of the indole NH due to the steric effects of the Cl substituent. Similarly, differences in H-bonding to the His 72 residue of the active site of TDO could, in part, explain the affinities that were measured. This study also leads to a better understanding of the mechanism of TDO inhibition by this chemical series from the structural and electronic points of view and the results obtained with the chloro-(2-pyridin-3-ylvinyl)-1*H*-indoles must now be extrapolated to the fluoro analogs of 680C91.

Author's contribution

LM wrote most of the manuscript and performed the structural (Crystallography, molecular modeling) and electronic analyses (dipolar moment, MEP). She also contributed to the determination of the solubilities of compounds. SL produced hTDO (overexpression and purification) and performed the enzymatic assays and IC_{50} determination. JR and ED performed the synthesis and chemical characterization of the compounds. MG and JMF supervised the enzymatic work. BM, RF and JW supervised and coordinated the chemical work.

Conflict of interest

None.

Acknowledgments

The authors thank Jérémy Maury who participated in the synthesis and crystallization of the compounds used in this study and Bernadette Norberg for assistance in the crystallographic part of the work. Financial contribution from the Fonds de la Recherche Scientifique-FNRS for the award of a Télévie grant to L. M. (7.4.543.07F) is greatly appreciated.

Appendix A. Supplementary data

Supplementary data related to this article can be found online at doi:10.1016/j.ejmech.2012.04.033.

References

[1] N.P. Botting, Chem. Soc. Rev. 24 (1995) 401–412.
[2] R. Schwarcz, Curr. Opin. Pharmacol. 4 (2004) 12–17.
[3] K. Schröcksnadel, et al., Clin. Chim. Acta 364 (2006) 82–90.
[4] D.J. Madge, et al., Biochem. Pharmacol. 49 (1995) 1435–1442.
[5] D.J. Madge, et al., Bioorg. Med. Chem. Lett. 6 (1996) 857–860.
[6] S.A. Rafice, et al., Biochem. Soc. Trans. 37 (2009) 408–412.
[7] M. Sono, et al., Chem. Rev. 96 (1996) 2841–2888.
[8] T.W. Stone, et al., Nat. Rev. Drug Discovery 1 (2002) 609–620.
[9] F. Forouhar, et al., PNAS 104 (2007) 473–478.
[10] Y. Kotake, et al., Physiol. Chem. 243 (1936) 237–244.
[11] J.M. Leeds, et al., J. Biol. Chem. 268 (1993) 17781–17786.
[12] J.B. Katz, et al., Immunol. Rev. 222 (2008) 206–221.
[13] O. Takikawa, et al., Adv. Exp. Med. Biol. 527 (2003) 277–285.
[14] L.A. Sanni, et al., Am. J. Pathol. 152 (1998) 611–619.
[15] A.L. Mellor, et al., Immunol. 13 (2001) 213–218.
[16] U. Grohmann, et al., Trends Immunol. 24 (2003) 242–248.
[17] D.H. Munn, et al., J. Clin. Invest. 117 (2007) 1147–1154.
[18] A.L. Mellor, et al., Nat. Rev. Immunol. 4 (2004) 762–774.
[19] S.J. Thackray, et al., Biochemistry 47 (2008) 10677–10684.
[20] C. Uyttenhove, et al., J. Nat. Med. 9 (2003) 1259–1274.
[21] S. Löb, et al., Nat. Rev. Cancer 9 (2009) 445–452.
[22] A.J. Muller, et al., Nat. Med. 11 (2005) 312–319.
[23] A.J. Muller, et al., Expert Opin. Ther. Targets 9 (2005) 831–849.
[24] A.J. Muller, et al., Curr. Cancer Drug Targets 7 (2007) 31–40.
[25] A. Macchiarulo, Amino Acids 37 (2009) 219–229.
[26] U. Röhrig, et al., J. Med. Chem. 53 (2010) 1172–1189.
[27] E. Dolušić, et al., Bioorg. Med. Chem. 19 (2011) 1550–1561.
[28] E. Dolušić, et al., Eur. J. Med. Chem. 46 (2011) 3058–3065.
[29] B. Van den Eynde, et al., WO2010008427 (2010).
[30] C.A. Opitz, et al., Nature 478 (2011) 197–204.
[31] L. Pilotte, et al., Proc. Natl. Acad. Sci. 109 (2012) 2497–2502.
[32] M. Civen, et al., J. Biol. Chem. 235 (1960) 1716–1718.
[33] N. Eguchi, et al., Arch. Biochem. Biophys. 232 (1984) 602–609.
[34] M. Salter, et al., Biochem. Pharmacol. 49 (1995) 1435–1442.
[35] M. Salter, et al., Neuropharmacology 34 (1995) 217–227.
[36] M. Salter, et al., Bioorg. Med. Chem. Lett. 6 (1996) 857–860.
[37] S.N. Young, Raven Press, New York, 1986, 49.
[38] E. Dolušić, et al., J. Med. Chem. 54 (2011) 5320–5334.
[39] G.M. Sheldrick, SHELX-97: Program for the Solution of Crystal Structures, University of Göttingen, Göttingen (Germany), 1998.
[40] A.L. Speck, University of Utrecht, Utrecht, The Netherlands, 2001.
[41] M.J. Frisch, et al., Gaussian 03. Revision B.04, Gaussian. Inc., Wallingford CT, 2004.
[42] E. Alegre, et al., Anal. Biochem. 339 (2005) 188–189.
[43] GraphPadPrism. Version 5.03, GraphPad Software, SanDiego CA, 2003.
[44] H.M. Berman, et al., Nat. Struct. Biol. 10 (2003) 980.
[45] Y. Zhang, et al., Biochem. 46 (2007) 145–155.
[46] C.L. Pierri, et al., Biochim. Biophys. Acta 1804 (2010) 1695–1712.
[47] S.F. Altschul, et al., Nucleic Acids Res. 25 (1997) 3389–3402.
[48] R. Lopez, et al., Nucleic Acids Res. 31 (2003) 3795–3798.
[49] SYBYL, Version 8.0, Tripos Inc., St. Louis, U.S.
[50] G. Jones, et al., J. Mol. Biol. 267 (1997) 727–748.
[51] M. Dixon, et al., Biochem. J. 55 (1952) 170–171.
[52] G.R. Desiraju, et al., in: , IUCr. Monographs on Crystallography, 9, 2001, p. 5.
[53] B.G. McGaughey, et al., J. Biol. Chem. 273 (1998) 15458–15463.
[54] J.P. Gallivan, et al., Proc. Natl. Acad. Sci. 96 (1999) 9459–9464.
[55] E. Salwińska, et al., Pol. J. Chem. 64 (1990) 813–817.
[56] A.R. Katritzky, et al., Cryst. Growth Des. 1 (2001) 261–265.